VARIABLE-SPEED GENERATORS WITH FLUX WEAKENING

A.A. Fardoun, E.F. Fuchs
Department of Electrical and
Computer Engineering
University of Colorado
Boulder, CO 80309

P.W. Carlin
National Renewable Energy Laboratory
Golden, CO 80401

ABSTRACT

A cost-competitive, permanent-magnet 20 kW generator is designed such that the following criteria are satisfied: an (over) load capability of at least 30 kW over the entire speed range of 60-120 rpm, generator weight of about 550 lbs with a maximum radial stator flux density of 0.82 T at low speed, unity power factor operation, acceptably small synchronous reactances and operation without a gear box. To justify this final design four different generator designs are investigated: the first two designs are studied to obtain a speed range from 20 to 200 rpm employing rotor field weakening, and the latter two are investigated to obtain a maximum speed range of 40 to 160 rpm based on field weakening via the stator excitation. The generator reactances and induced voltages are computed using finite element/difference solutions. Generator losses and efficiencies are presented for all four designs at rated temperature of $T_r=120^\circ C$.

INTRODUCTION

Most generator choices for wind turbines sized in the 50-3000 kW range are of the synchronous, squirrel-cage induction and wound-rotor induction machine type. These generators have limitations on speed range (constant, or $\pm$ 20%), and some have a relatively low power factor (e.g., p.f. < 0.9) on the machine and power system sides of the plant [1,2]. Others attempt to increase the speed range by operating a wound-rotor induction machine as a doubly fed generator [3]; the cost and complexity of this type make it undesirable. Also, current harmonics on the power system side are not controlled which degrade the quality of power, therefore, requiring passive filters and power factor correction capacitors. Moreover, all wind generators that have been built rely heavily on gear boxes. Since the gear box of a wind power plant needs to be maintained at appreciable cost about every five years [4], and is an expensive part of a wind power system, it would be advantageous to build a plant without one.

In Figure 1, a novel variable-speed wind power train is introduced. It will have the following characteristics:
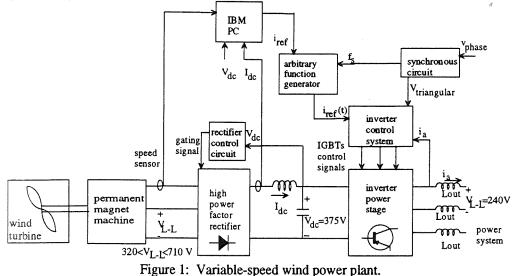A permanent-magnet machine (PMM) with a speed range of 60-120 rpm with minimum weight, size and number of poles. A newly developed buck-type rectifier [5] --which maintains a high power factor as well as a low total harmonic current distortion-- utilizing only one active switch will be used to rectify the generator output voltage. The dc voltage will then be converted to ac via an inverter. The output inverter current is controlled to produce a desired power factor as well as any desired harmonic content and thus acts as an active filter. In addition, the inverter current will be controlled such that noninteger harmonics do not exist and selected harmonics are eliminated to prevent resonance phenomena.

Since PMMs have inherent advantages over induction and synchronous machines --such as higher efficiency, no brushes, no excitation losses and no field coils or virtually no rotor losses [6]-- a permanent-magnet generator is chosen for this wind power plant application. Four different permanent-magnet machine designs generating a minimum no-load voltage of $V_{L-L}=\sqrt{3}\cdot185$ V= 320.4 V, are explored. The speed range for these machines varies from 60-120 rpm (design #3) to 20-200 rpm (design #2). The main objective of this paper is to investigate and design a PMM for wind power applications. The PMM should generate 1.5 times the rated output power over the desired speed range. To produce the maximum real output power the machine is operated at unity power factor. To approximately optimize the PMM design, the "chosen" configuration is compared with three other designs having different speed ranges and control schemes. A comparison of the four designs based upon magnet costs (volume), efficiency, weight and machine size is performed.

DESIGN OF 20 kW GENERATOR WITH FLUX WEAKENING

Two alternative three-phase permanent-magnet machine types for the generator design are considered. In the first one the flux weakening is achieved via an additional rotor coil counteracting the permanent-magnet excitation as speed increases. For this type two alternative designs (design # 1 and design # 2) are compared. The reason for studying two different designs is to investigate the possibility of a machine with a 1:10 speed range.

These designs differ in the location of the permanent-magnet as explained later. In the second type the flux weakening is controlled via field orientation of the stator excitation; no rotor coils are needed resulting in a less expensive and lighter machine. Again two alternative designs (design # 3 and design # 4) are investigated. For both designs no limits are set neither for the flux weakening nor the speed range, however, they are investigated in a way to explore the maximum possible speed range within the given limits of the terminal voltage. Designs 3 and 4 differ in the field orientation of the stator current. In design # 3 the stator current distribution is controlled to produce a unity power factor without weakening but strengthening the permanent-magnet excitation; while in design # 4 the stator current distribution is controlled to weaken the permanent-magnet excitation disregarding the unity power factor constraint. Because neodymium-iron-boron permanent-magnet material has a larger coercivity and a greater energy product than other permanent-magnet materials and thus a higher power/weight ratio [6], it is used for this generator. Since the machine speed is proportional to the phase voltage (Eq. 1), using flux weakening will bound the terminal voltage (V_t) to $V_{rated} \leq V_t \leq 2 \cdot V_{rated}$; where V_{rated} is the rated generator phase voltage at low speed.

Figure 1: Variable-speed wind power plant.

$$E_{rms} = 4.44 \cdot N_{ph} \cdot f \cdot \varphi_{Fe} B_{maxw} \cdot k_w \cdot 1 \cdot \tau_p, \qquad (1)$$

where N_{ph} is the number of series turns per phase of the stator winding, f is the frequency of the machine current and voltage (e.g., f=4 Hz at speed of 20 rpm), φ_{Fe} is the iron stacking factor =0.9, B_{maxw} is the maximum (fundamental) stator radial flux density at the radial center of the stator winding, k_w is the pitch factor, 1 is the actual machine length, τ_p is the pole pitch length=$2\pi R_{sw}/P$, where P is the number of poles and R_{sw} is the stator radius at the radial center of the stator winding.

All designs have common constraints derived from the minimum (rated) output voltage of the machine (Figure 1).

Design Constraints

The generator design is based on the following constraints:

output power: $P_{out} = 20$ kW,

line-to-neutral voltage at no load: $V_{L-N} = 185V$

base impedance: Z_{base}=5.14Ω,

current density:3.8 < J < 5 A/mm^2

copper fill factor: 0.5 < k_s< 0.75

winding pitch: k_w=1.0 (full pitch),

overload capacity: P_{max} >1.5 P_{rated} over the desired speed range,

synchronous quadrature and direct-axis reactance at low speed: X<1.0 p.u.,

no gear box, forced ventilation, drip-proof,

terminal voltage limited to $V_{rated} \leq V_t \leq 2 \cdot V_{rated}$ over desired speed range,

maximum rated temperature: T_{rated}=140^{0}C.

Generator Design: Type # 1

For this type two alternative designs are considered. The first one, design # 1, has permanent magnets mounted on the surface of the rotor pole shoes and the flux weakening coil is located --like in the case of a

conventional synchronous machine-- in the interpolar rotor space (Figure 2a). The second design, design # 2, has permanent magnets mounted within the rotor yoke and the flux weakening coil is located in the interpolar space as for design # 1 (Figure 2b). However, the flux weakening coil lies between the stator winding and the permanent-magnet excitation for design # 2 while for design # 1 the permanent magnet lies between the stator winding and the flux weakening coil.

From a linear analysis point of view -neglecting saturation and leakage effects- both designs are the same. However it has been shown in [7] that design # 2 provides a wider speed range than design # 1 due to the nonlinear behavior of the machine caused by saturation and leakage. Since the linear analysis neglects iron-core saturation and the leakage flux of the machine, its validity is severely limited. The linear approach will reveal linear flux weakening characteristics, while the nonlinear analysis, based on numerical solutions (e.g., finite element/ difference techniques), indicates that the characteristics are nonlinear.

Numerical magnetic field solutions for the generator cross-section are obtained with an available finite element/difference software program. This software is modified to permit the modeling of permanent-magnet machines. The magnet is approximated by thin current sheets along both sides of the permanent magnet [8]; the magnet behaves almost like an air gap with a permeability of $\mu_m=1.06\mu_0$. The flux weakening coils (ampere-turns) are assumed to be uniformly distributed within the rotor slot and modeled by inputting the desired ampere-turns in the rotor slot (Figure 2a). In addition, inputs to the field calculation program are the magnetic characteristics (e.g., iron-core characteristics, magnet height, coercivity and flux weakening current) and the geometric dimensions of the machine. The output consists of the vector potentials and the radial flux density of the machine within one pole pitch. Given the flux density in the radial center of the stator, the PMM phase voltage is computed using Eq. 1.
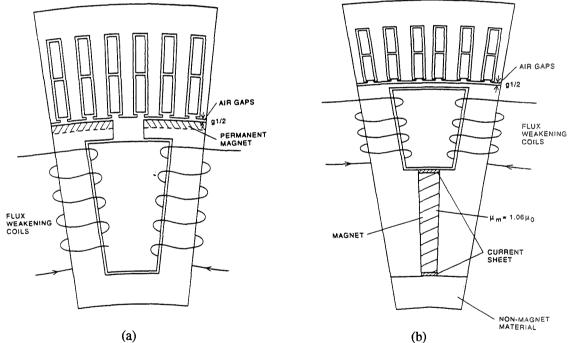

Figure 2: Geometric dimensions of designs # 1 (a) and # 2 (b).

Design # 1: For design # 1 the permanent magnets of the machine are mounted on the surface of the rotor pole shoes as shown in Figure 2a. The flux weakening characteristics at no load and full load are computed via finite element/difference method. Figures 3a, b illustrate flux distributions of design # 1 at full load for flux weakening of -500 and -6700 AT, respectively. Flux weakening at no load is possible down to about $B_{maxw}=0.3$ T and at full load down to 0.45 T. The flux weakening current cannot be increased because the permanent magnet might be demagnetized. Figure 4 presents the flux weakening characteristics of the PMM versus speed and B_{maxw} for design # 1 at full load. In this figure B_{maxw} is the maximum radial flux density within the radial center of the stator winding and $(AT)_{FW}$ are the total ampere turns of the flux weakening coil within one rotor slot. Since the flux weakening coil is not situated in between the stator winding and the permanent magnet,

armature reaction and leakage flux effects limit the flux density reduction to 0.45 T and one achieves a speed range of 1:4.

Design # 2: In design # 2 the permanent magnet is placed within the rotor yoke as shown in Figures 2b. In this configuration the flux weakening coil lies in between the stator winding and the permanent magnet. Nonlinear numerical solutions show that this location of the magnet makes it possible for the flux weakening coil to reduce the radial flux density in the stator to virtually zero at no load condition and to 0.2 T at full load. Figures 3c, d show flux distributions for design # 2 at full load for speeds of 20 and 200 rpm, respectively. Computed characteristics at full load are given for design # 2 in Figure 4. It should be noted that as flux weakening increases the value of the quadrature reactance (X_q) increases as explained in [7].
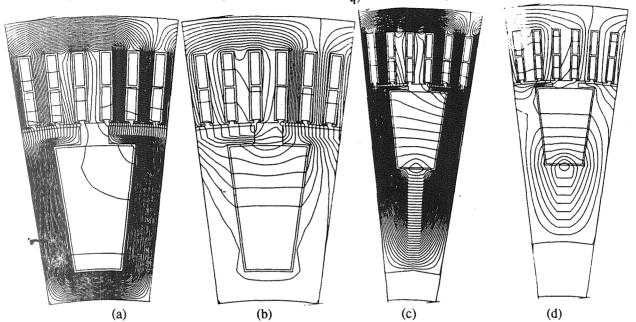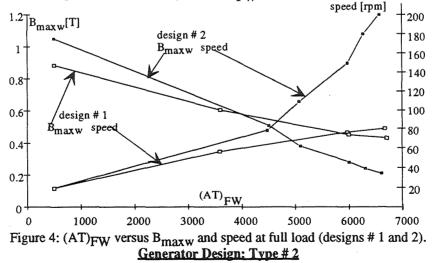

(a) (b) (c) (d)

Figure 3: Field distribution for design # 1 at full load for (a) n=20 rpm at $(AT)_{FW}$=-500 AT, (b) n=80 rpm at $(AT)_{FW}$=-6700 AT, and design # 2 for (c) n=20 rpm at $(AT)_{FW}$=-500 AT, (b) n=200 rpm at $(AT)_{FW}$=-6600 AT .

Figure 4: $(AT)_{FW}$ versus B_{maxw} and speed at full load (designs # 1 and 2).

Generator Design: Type # 2

In this type flux weakening is controlled by varying the phase angle of the stator magnetomotive force (mmf) with respect to the rotor excitation. Two alternative designs (designs # 3 and 4) are investigated. The magnet excitation is weakened by controlling the phase angle of the stator mmf and the amplitude of the stator current such that the output power is equal to or greater than 20 kW.

Design # 3: In design # 3 the stator current is controlled such that it is in phase with the stator voltage (unity power factor operation). The permanent-magnet excitation is not opposed, on the contrary the flux density in the air gap increases due to the stator current distribution which reinforces the permanent-magnet mmf as

356

shown by the phasor diagram. Because the voltage increases due to the strengthening of the mutual flux by the stator mmf, the machine current is below its rated value. This results in a reduction of the stator slot size and therefore weight. Since the flux density is not decreased (no flux weakening), the speed is limited to a 1:2 range because the terminal voltage is limited by the same ratio to $V_{rated} \leq V_t \leq 2 \cdot V_{rated}$. To maintain a constant output power, the machine current is decreased at high speed to half the current value at low speed since the voltage increases by a factor of 2 at high speed. Hence, the losses at high speed are less than those at low speed. It is also important to note that the weight of this machine is significantly smaller than those of type # 1 due to the fact that no flux weakening is applied and no rotor coils are used. Since this design is less expensive --as the number of poles decreases, it will be easier to manufacture and the magnet volume decreases-- it will be investigated for 12, 16, 20, and 24 poles. However, the number of stator turns increases in order to guarantee the minimum no-load voltage. The cost, weight, efficiency, magnet volume and machine reactances for 12, 16 and 20 poles are presented in Table 1.

Full-Load Analysis: The performance of design # 3 at full load is investigated using a finite element/difference software. The machine load is modeled by the stator current and the angle ψ [7], which is the angle between the stator mmf F and the fictitious induced voltage $\tilde{E}_o$. Since one of the constraints for this design is to operate at unity power factor load ($\theta=0$) ψ is equal to the torque angle δ. The phasor diagram at n=60 rpm is presented in Figure 5. Note that the quadrature machine reactance X_q can be computed using the phasor diagram. Both the reactances determined from flux linkages and those obtained from the phasor diagram match very well.

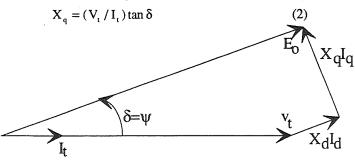$$X_q = (V_t / I_t) \tan \delta \qquad (2)$$

Figure 5: Phasor diagram for speed of n=60 rpm.

Flux distributions for design # 3 at no load and full load at n=60 rpm are shown in Figure 6a and 6b, respectively. As mentioned before, due to the stator current excitation which strengthens the permanent-magnet mmf resulting in a higher radial flux density at unity power factor load than at no load. The strengthening of the mutual flux increases the flux density B_{maxw} to about 0.82 T (from 0.63 T at no load). This is fortuitous since the utilization of the machine increases with increasing stator load currents; or in other words the no-load induced voltage is always somewhat smaller than the induced voltage at any load at unity power factor.

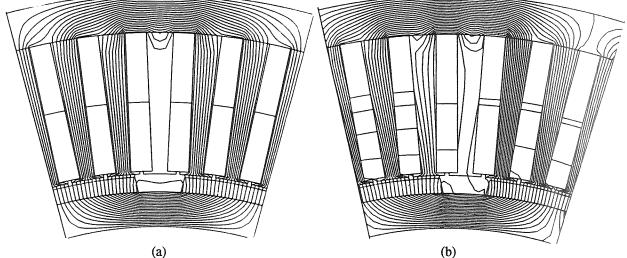(a)   (b)

Figure 6: Flux distribution for design # 3 (a) at no load and (b) full load n=60 rpm.

<u>Calculation of Direct and Quadrature Synchronous Inductances:</u>   The direct (L_d) and quadrature (L_q) inductances of one phase of the stator winding of the machine are defined as

$$L_d = L_{md} + L_{dl} + L_{de} \text{ and } L_q = L_{mq} + L_{ql} + L_{qe}, \qquad (3a, b)$$

where L_{md}, L_{dl} and L_{de} are the mutual, leakage and end leakage direct inductances, respectively; L_{mq}, L_{ql} and L_{qe} are the mutual, leakage and end leakage quadrature inductances. Note that all inductance values for the direct and quadrature inductances are computed using the same flux linkage method explained below, except that $\psi = 90^\circ$ for L_d while $\psi = 0^\circ$ for L_q.

   Synchronous Self Inductance without L_e: The synchronous inductance is computed using the flux-linkage method [9]

$$L = \Psi / I, \qquad (4)$$

where Ψ are the flux linkages per phase and I is the current in one turn.   The flux linkages are approximated as the sum of the flux linkages of the top and bottom layer coil sides of a phase belt. The flux linkages of a top (t) coil side with N_c turns (see Figure 7) are

$$\Psi^t = N_c \cdot A^t_{sm\tau} \cdot 1 \cdot \varphi_{Fe}, \qquad (5)$$

where $A^t_{sm\tau}$ is the vector potential at the center of the $m\tau^{th}$ coil side of the top layer of the stator winding. The

vector potentials $A^t_{sm\tau}$ are computed from incremental magnetic stator field distributions existing at a given load: the reluctivities obtained for a given operating point (e.g., full load) are maintained constant that is "frozen" and are used for the calculation of the synchronous inductance of one stator phase. The inductances of the top and bottom coil sides of phase B of the stator winding can be approximated as defined in Figure 7 and described by Eqs. 6a and 6b, respectively.

$$L^t = \frac{1}{I^t_B} \sum_{m\tau=1}^{M\tau} N_c \cdot 1 \cdot \varphi_{Fe} \cdot A^t_{sm\tau B}, \qquad (6a)$$

and

$$L^b = \frac{1}{I^b_B} \cdot \sum_{m\tau=1}^{M\tau} N \cdot 1 \cdot \varphi_{Fe} \cdot A^b_{sm\tau B}, \qquad (6b)$$
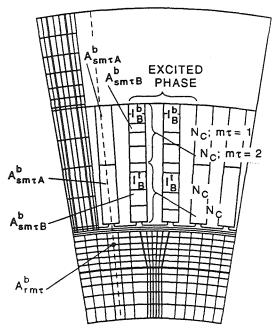

Figure 7: Definition of the stator self inductance for $M\tau = 2$.

where $M\tau$ is the number of coils per pole, $A_{sm\tau B}^{b}$ is the vector potential at the center of the $m\tau^{th}$ bottom layer coil side of the stator winding of phase B and I_{B}^{t} is the current in one turn of the coil side. The sum of Eqs. (6a) and (6b) is the inductance of a phasebelt L^{i} for i=A, B and C. The direct (X_d) or quadrature (X_q) reactance of a phase can now be computed as

$$X_s = 2\pi f \cdot \beta (L^A + L^B + L^C) / \alpha \cdot m_s, \qquad (7)$$

where β is the number of phasebelts in series which is equal to the number of poles P for the connection at hand, α is the number of phasebelts in parallel which is 1 for the given application, and m_s is the number of stator phases. The direct and quadrature synchronous reactance values per phase of the machine are listed in Table 1.

Armature Leakage Reactances: The leakage flux linkages are computed using Eq. 4. Since the flux linkages for the leakage inductance are those that link the stator and do not link the rotor (see Figure 7), Equation 5 is modified as

$$\Psi_1 = N_c \cdot 1 \cdot \varphi_{Fe} (A_{sm\tau}^{t} + A_{sm\tau}^{b} - 2A_{rm\tau}), \qquad (8)$$

where Ψ_1 are the total flux linkages (top and bottom coils) for the leakage inductance, $A_{sm\tau}^{t}$ and $A_{sm\tau}^{b}$ are the vector potentials within the top and bottom layers of the $m\tau^{th}$ coil in the stator and $A_{rm\tau}$ is the corresponding rotor vector potential as shown in Figure 7. Again $\psi=90^0$ for L_{dl} while $\psi=0^0$ for L_{ql}. Assuming that the top and bottom layers of the stator coil (phase B) have the same current the leakage inductance corresponding to phase B is

$$L_1 = \frac{1}{I_B} \sum_{m\tau=1}^{M\tau} N_c \cdot 1 \cdot \varphi_{Fe} (A_{sm\tau B}^{b} + A_{sm\tau B}^{t} - 2A_{rm\tau}). \qquad (9)$$

The leakage reactance is computed using Eq. 7. Typical leakage reactances at low speed for design # 3 are listed in Table 1. Figures 8a, and 8b represent field distributions for the calculation of direct and quadrature synchronous inductances as well as the armature leakage inductance.

Armature End Leakage Reactance: The end leakage reactances are approximated as

$$L_{de}=L_{dl}/3 \qquad (10a)$$

and

$$l_{qe}=L_{ql}/3. \qquad (10b)$$

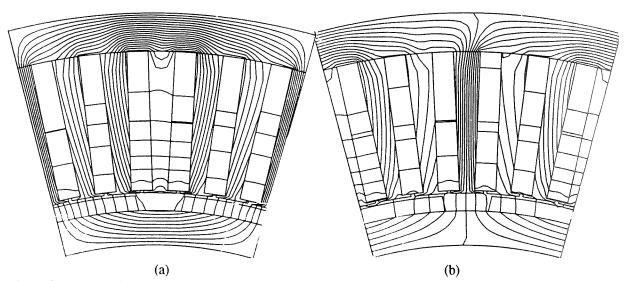(a)   (b)

Figure 8: Field distribution for the calculation of (a) the saturated direct synchronous inductance L_d and armature leakage inductance L_{dl} (design # 3, 12 poles) and (b) saturated quadrature synchronous inductance L_q and armature leakage inductance L_{ql} (design # 3, 12 poles).

Power Calculation: The output power of the generator can be determined in two alternative ways : first from

$$P_{out} = 3V_t I_t \cos\theta,\qquad(11)$$

and

$$P_{out} = 3(\frac{E_o V_t}{X_d}\sin\delta + \frac{X_d - X_q}{2X_d X_q}V_t^2 \sin 2\delta).\qquad(12)$$

The results of both approaches corroborate quite well. The output power versus the torque angle δ characteristics are shown in Figure 9 for speeds of 60 and 120 rpm.

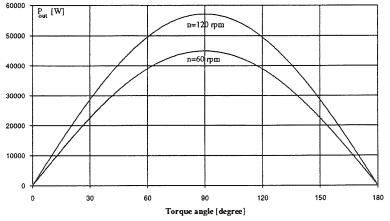
Figure 9: Power versus torque angle characteristics at low and high speeds (design # 3).

Table 1: Comparison of cost for design # 3 with 12, 16 and 20 poles.

# of poles	12		16		20	
speed [rpm]	60	120	60	120	60	120
magnet volume per pole [cm^3]	112.2		109.8		90.9	
weight [lbs.]	537		570.7		511	
# of turns per phase per pole	32		18		14	
total losses [W]	1846	730.3	2939.9	1139.3	2637.4	1096.5
ohmic losses [W]	1795	586.2	2856.6	903.5	2533.1	801.5
core losses [W]	51	144.1	83.3	235.8	104.3	295
efficiency [%]	90.8	96.3	85.3	94.3	86.8	94.5
radial flux density [T]	0.818	0.709	0.776	0.713	0.764	0.714
L-N voltage [V]	235.9	408.9	207.5	381	203.8	379
phase current [A]	28	16	32	18	32	18
d-axis reactance [Ω]	3.36	6.71	2.1	4.2	1.55	3.1
d-axis leakage reactance [Ω]	1.16	2.32	0.7	1.4	0.6	1.2
q-axis reactance [Ω]	2.51	3.02	1.7	3.4	1.45	2.9
q-axis leakage reactance [Ω]	1.09	2.18	0.68	1.36	0.55	1.1

Design # 4: In this design the permanent-magnet excitation is weakened by controlling the relative position of the stator mmf with respect to the rotor mmf so that the stator mmf opposes that of the permanent magnet as shown in the phasor diagram of Figure 10. Controlling the air gap flux via the stator excitation requires a six-switch rectifier instead of one switch as proposed for designs # 1, 2 and 3. Even though this machine has no flux weakening rotor coil losses, its stator conduction losses increase because the stator current is increased as the speed increases to weaken the flux. It also should be noted that the weight of this machine is less than those of machines of designs # 1 and # 2. However, the speed range of this configuration is limited to 1:4 while that of design # 2 is from 1:10.
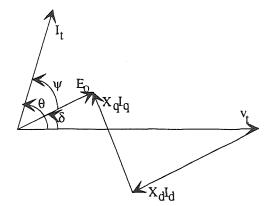
Figure 10: Phasor diagram for design # 4 at n=160 rpm.

DESIGN CONSIDERATION FOR 300 kW GENERATOR

The weight of the 20 kW machine is approximated as

$$W_{20kW} = \varphi_e \pi (R_{so}^2 - R_{ri}^2) l \gamma_{Fe}, \tag{13}$$

where φ_e is a filling factor and γ_{Fe} is the iron specific weight. Model laws for electrical machines indicate that the output power P_{out} of a machine relates to the dimension X as $P_{out} \alpha\ (X)^4$ while the volume (weight) of a machine increases according to $W \alpha\ (X)^3$. Since the present 20 kW is somewhat overdesigned one can extract at least 30 kW from the present volume (or weight) and therefore a 300 kW machine will weigh

$$W_{300kW} = W_{20kW} \cdot 10^{3/4} \tag{14}$$

The approximate weights for all four machine designs is listed in Table 2. However, it should be noted that it is difficult to mount the rotor of a permanent-magnet machine of 300 kW (designs 1, 3 and 4). An alternative solution is to locate the magnet within the rotor yoke as employed for design # 2, where the permanent magnets can be installed after the rotor has been mounted.

DISCUSSION AND CONCLUSIONS

Four machine designs are investigated; the first one is not recommended because design # 2 has a wider speed range with almost the same weight and efficiency. Therefore, the task remains to choose one machine from the remaining three designs for construction and testing. Table 2 lists magnet costs (magnet size), machine weights as well as efficiencies and losses. One should also consider that this application deals with wind turbines as prime movers. In practice about 80 % of the available wind energy is extracted by wind turbines with constant-speed generators [4]. With a machine of a speed range of 1 to infinity one could extract the remaining 20 %. However, a machine with a speed range of 1 to 2 (e.g., 60-120 rpm) one can extract about 18% of the available 20% [4]. This fact leads to the simple conclusion that design # 3 is the most cost-competitive design for wind power plants. Note that design # 3 with 12 poles is chosen for construction since it has 72 stator slots and the appropriate laminated core is an off-the-shelf item; in other words it is the least expensive among the 12, 16 and 20 pole configurations. The efficiency of the 12 pole arrangement is the highest among all other designs. Efficiencies for all four designs are shown in Figures 11. Note that the efficiency for design # 3 increases as the speed increases because the current decreases and the voltage increases maintaining constant output power without applying any flux weakening. Efficiencies for designs 1 and 2 are maximum around n=40 rpm since the terminal voltage is assumed to increase from 20 rpm to 40 rpm and the current is allowed to decrease and thus the stator losses decrease. At high speeds the losses increase due to the high rotor losses even though the stator losses decrease due to lower stator current. For design # 4, the stator losses increase at high speed since the stator current is increased to weaken the machine radial flux density. The temperature in all generators is assumed to be 120 °C and the conduction losses are increased accordingly. The magnet size for designs # 1 and 2 is adjusted assuming that the magnet temperature is 140 °C while for designs # 3 and 4 it is sized such that the magnet temperature is 120 °C. It should be mentioned that the performance of design # 4 for different pole numbers has not been researched, however, this will not change the validity of the above conclusion for choosing design # 3 as the most cost-competitive design for this wind power plant application.
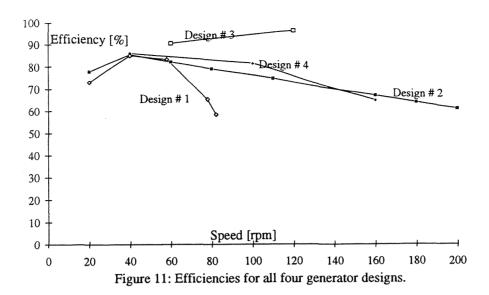
Figure 11: Efficiencies for all four generator designs.

Table 2: Comparison of cost, weight and efficiency of all four designs.

	Design # 1	Design # 2	Design # 3	Design # 4
# of poles	24	24	12	24
magnet volume per pole [cm^3]	92.	231.1	112.2	67.
weight [lbs]	1286	1584.	537	638.3
weight of 300 kW machine [lbs.]	7231.7	8907.5	3019.8	3589.4
speed range [rpm]	20-85	20-200	60-120	40-160
high speed efficiency [%]	58.6	61	96.3	64.3
total high speed losses [W]	8288	7796.2	730.3	7059.8
high speed stator losses [W]	1218	1013.1	586.2	6504.8
high speed rotor losses [W]	7070	6783.1	144.1	555
low speed efficiency [%]	73	77.7	90.8	86.5
total low speed losses [W]	5408.2	4452	1846	2703.6
low speed stator losses [W]	5366.2	4410	1795	2634.3
low speed rotor losses [W]	42	42	51	69.3
energy flow	one direction	one direction	one direction	both directions

REFERENCES

[1] T. H. Lauw, "AC-DC-AC Conversion Systems for Mains-Connected Windpower Generation", ASME Wind Energy Symposium, 1988.

[2] E. Hinrichsen, "Variable Rotor Speed for Wind Turbines, Objectives and Issues", Windpower, San Francisco, CA, 1985.

[3] P. Holmes and N. Elsonbatty, "Cycloconverter-Excited Divided-Winding Doubly-Fed Machine as a Wind-Power Converter", IEE Proceedings-B, Vol. 131, March 1984, pp. 61-68.

[4] C. P. Butterfield, W. Musial and P. W. Carlin, National Renewable Energy Laboratory, private communication, June 1992.

[5] E. Ismail and R. W. Erickson, " A Single Transistor Three Phase Resonant Switch for High Quality Rectification", IEEE Power Electronic Specialist Conference, Spain, July 1-7, 1992, pp. 1341-1351.

[6] P. Mellor, B. Chaaban and K. Binns," Rare Earth Permanent-Magnet Motors Avoiding Measurement of Load Angle", IEE Proceedings-B, Vol. 138, No. 6, 1991, pp. 322-330.

[7] E. F. Fuchs, A. A. Fardoun, P. Carlin and R. W. Erickson, "Permanent Magnet Machines with Large Speed Variations", American Wind Energy Association Conference, Seattle, 19-23 October, 1992.

[8] J. R. Brauer, L. A. Larkin and V. D. Overbye, "Finite Element Modeling of Permanent Magnet Devices", Journal of Applied Physics, Vol. 55, pp. 2183-2185, March, 1984.

[9] E. F. Fuchs, M. Poloujadoff and G. W. Neal, " Starting Performance of Saturable Three-Phase Induction Motors", IEEE Trans. on Energy Conversion, Vol. 3, No. 3, September 1988, pp. 624-633.